2024 American Control Conference (ACC)
July 8-12, 2024. Toronto, Canada

Weaknesses and Improvements of the Extended Kalman Filter for Battery State-of-Charge and State-of-Health Estimation

Shida Jiang[1], Junzhe Shi[1], Manashita Borah[1,2], and Scott Moura[1]

Abstract— **Battery management systems (BMS) are essential for ensuring battery performance and safety. Accurate estimation of the State of Charge (SOC) and State of Health (SOH), for example, are critical. However, utilizing the conventional Extended Kalman Filter (EKF) for SOC and SOH co-estimation is often challenging due to problems such as overconfident covariance estimation, overly simplistic assumptions about process noise and measurement noise covariance matrices, and the shift of the open circuit voltage (OCV) curve as the cell ages. To address these issues, this paper introduces an improved EKF design for co-estimating the SOC and SOH. The proposed approach incorporates innovative strategies to counteract covariance pitfalls, calculates the optimal covariance matrix configuration objectively, and incorporates OCV shifts from aging. Comparative simulations underscore the superiority of our method against traditional EKF and Unscented Kalman Filter (UKF) techniques. The code is available at `https://github.com/Shida-Jiang/EKF_UKF_SOCSOH_estimation`.**

I. INTRODUCTION

A. Background and Motivation

Battery management systems (BMS) are integral to ensuring battery longevity, reliability, and safe operation across diverse applications, ranging from electric vehicles to renewable energy storage systems [1]. Central to these systems is estimating the State of Charge (SOC) and State of Health (SOH) [2], which cannot be directly measured. The SOC quantifies the battery's remaining capacity (current energy level) as a percentage of its current maximum capacity, while the SOH provides insight into the battery's aging condition. The SOH typically expresses the current maximum capacity as a percentage of the battery's initial maximum capacity [3]. Accurate estimations of both SOC and SOH are paramount. They ensure efficient energy utilization, extend battery lifespan, and bolster operational safety [4]. With these considerations in mind, the primary goal of this study is to design an optimal and robust algorithm for the co-estimation of SOC and SOH.

B. Literature Review

The Extended Kalman Filter (EKF) has gained prominence in numerous state estimation applications because of its proficiency in handling nonlinear systems [5]. Nonetheless, it is not free from challenges. A notable limitation of the EKF is its susceptibility to rapid covariance drops, especially in scenarios characterized by complex nonlinear dynamics [6]. While a swift decline in covariance can signify high confidence in state estimates, it is a double-edged sword. Such rapid drops can lead to overconfident estimations, posing issues, particularly in contexts where exact state predictions are crucial [7]. Overconfidence in the predictions can render it less adaptable to new, unforeseen data, ushering in an over-optimism dilemma. This shortcoming becomes especially pronounced in BMS, where precise state estimation is pivotal to operational safety and efficiency.

While the EKF is fundamentally an approximation of the Bayesian state estimator and lacks universal convergence guarantees, it has been effectively applied across various practical applications. Its appeal largely stems from its lower computational burden compared to other estimators, such as the Unscented Kalman Filter (UKF) [8] and the Iterated Extended Kalman filter (IEKF) [9]. Numerous studies have leveraged the EKF for simultaneous battery SOC and SOH estimation. For instance, Plett utilized extended Kalman filters to estimate both the states and parameters of a battery's electrical circuit model (ECM) [10]. Similarly, Xu and colleagues introduced an adaptive dual EKF approach for SOC and SOH co-estimation [11]. However, many of these studies often gloss over the intricate setup of the noise covariance matrix within the EKF framework specific to co-estimation and simply assume that the noise covariance matrix is a constant and diagonal matrix [12]. Neglecting this aspect can compromise the accuracy and reliability of the resultant estimates.

Beyond the research gaps mentioned earlier, it is essential to delve deeper into the nuanced relationship between the SOH and open circuit voltage (OCV) of a battery, often characterized as the OCV shift. In the literature, many algorithms tasked with battery state estimation lean heavily on the SOC-OCV relationship, assuming that this relationship remains static [13]. However, this assumption can sometimes lead to a significant error in SOC and SOH estimation, as changes in SOH can directly modify the OCV curve, thereby altering the intrinsic dynamics of the battery [14]. The OCV curve shift embodies a complex interplay of various chemical and physical processes inside the battery, such as changes in the solid electrolyte interphase (SEI) and electrode degradation [15]. While initial shifts may seem minimal, their aggregated impact, particularly as they intensify with time, can markedly affect both the battery's performance and the precision of its state estimation [16].

*M. Borah in this work is supported by Fulbright fellowship grant and SAFT.

[1]Shida Jiang, Junzhe Shi, Manashita Borah, and Scott Moura are with the Department of Civil and Environmental Engineering, University of California, Berkeley, CA, 94720 USA. shida_jiang@berkeley.edu, junzhe@berkeley.edu, manashitaborah@berkeley.edu and smoura@berkeley.edu. [2] Manashita Borah is also with Department of Electrical Engineering, Tezpur University, Assam, India, 784028

C. Contributions

This paper extends the existing research by designing an improved EKF for SOC and SOH co-estimation that addresses several critical weaknesses. In summary, the contributions and novelties of this study are as follows:

- A new technique to address the inherently inaccurate covariance estimation in traditional EKF. This technique ensures a more consistent and reliable confidence interval estimation.
- A methodology to more accurately model the noise covariance matrix in the EKF framework specifically tailored for battery SOC and SOH co-estimation. This approach seeks to bolster the robustness and accuracy of the EKF.
- Experimental data on the OCV shift due to SOH variations is collected. Using these empirical data, we built the EKF algorithm in a way that enables us to integrate this OCV shift into the SOC and SOH estimation process.

D. Structure of the Paper

The structure of this paper is delineated as follows: Section II delves into the methodology employed in our study. Section III presents simulation results, utilizing two distinct current profiles, and offers a comparative analysis between our proposed method and the traditional EKF and UKF approaches. Section IV provides a comprehensive summary and conclusion of our findings.

II. METHODOLOGY

A. Conventional Extended Kalman Filter Algorithm and its Weaknesses

The conventional EKF algorithm built for the nonlinear model represented by (1) is summarized in Algorithm 1. To adapt to the nonlinear state transition function and measurement function, EKF linearizes the two functions at each step and estimates the covariance based on the linearized functions.

$$\begin{cases} \boldsymbol{x_k} = f(\boldsymbol{x_{k-1}}, u_k) \\ z_k = h(\boldsymbol{x_k}, u_k) \end{cases} \tag{1}$$

While linearization (first-order approximation) is a commonly used technique when dealing with nonlinear systems, we found that linearization performed in the EKF, especially the linearization of the output function, can make the covariance estimation inaccurate. To better illustrate this, an example is shown below.

Consider two simple two-state systems S_1 (represented by (2)) and S_2 (represented by (3)). The two systems have the same state-space function and start with the same initial states $[x_{1,0}, x_{2,0}]^T = [1, 0.99]^T$ and initial covariance matrix $P_0 = I_{2\times 2}$. Both systems have zero process noise and a measurement noise of 1e-8. The measurement at each step is always $z_k = 2$.

$$\begin{cases} \begin{bmatrix} x_{1,k} \\ x_{2,k} \end{bmatrix} = \begin{bmatrix} x_{1,k-1} \\ x_{2,k-1} \end{bmatrix} \\ z_k = 2x_1 + x_2 - 1 \end{cases} \tag{2}$$

Algorithm 1 The extended Kalman filter algorithm

Inputs: $\boldsymbol{x_0}, P_0, u_k, z_k$

$k \leftarrow 0$

while $k < length(\boldsymbol{u})$ **do**

$k \leftarrow k + 1$

State prediction $\boldsymbol{x_{k|k-1}} \leftarrow f(\boldsymbol{x_{k-1}}, u_k)$

Calculate the state transition matrix $F_k = \frac{\partial f}{\partial x}|_{x=x_{k|k-1}}$

Calculate the process noise Q_k

Covariance prediction $P_{k|k-1} \leftarrow F_k P_{k-1|k-1} F_k^T + Q_k$

Calculate the residual $y_k \leftarrow z_k - h(\boldsymbol{x_k}, u_k)$

Calculate the measurement Jacobian matrix $H_k \leftarrow \frac{\partial h}{\partial x}|_{x=x_{k|k-1}}$

Calculate the measurement noise R_k

Calculate the Kalman gain $K_k \leftarrow \frac{P_{k|k-1} H_k^T}{H_k P_{k|k-1} H_k^T + R_k}$

State update $\boldsymbol{x_{k|k}} \leftarrow \boldsymbol{x_{k|k-1}} + K_k y_k$

Covariance update $P_{k|k} \leftarrow (I - K_k H_k) P_{k|k-1}$

Output $\boldsymbol{x_k}, P_k$

end while

$$\begin{cases} \begin{bmatrix} x_{1,k} \\ x_{2,k} \end{bmatrix} = \begin{bmatrix} x_{1,k-1} \\ x_{2,k-1} \end{bmatrix} \\ z_k = x_1^2 + x_2 \end{cases} \tag{3}$$

Neither system is observable in the linear system sense, and the only difference between them is that the first system has a linear output function, while the second system has a nonlinear output function. When a KF is used to estimate the states (which are actually two parameters since their values never change) of the first system, the state estimates converge at $[x_1, x_2]^T = [1.004, 0.992]^T$. The covariance matrix will converge to a constant matrix, which is $P = \begin{bmatrix} 0.2 & -0.4 \\ -0.4 & 0.8 \end{bmatrix}$. This result is reasonable because the measurement function only tells us that the actual state lies somewhere on the line $2x_1 + x_2 - 1 = 2$ but does not tell us the exact location. The nonzero covariance matrix P shows that the KF remains reliable when the system is unobservable and is aware that the estimation can be inaccurate under such a condition.

However, things are different for the second system. Since the system has a nonlinear output function, we use an EKF to estimate the states. After several iterations, the state estimation will converge at approximately the same point, which is $[1.002, 0.996]^T$. However, the covariance matrix will converge to a very small matrix $P = \begin{bmatrix} 0.0003 & -0.0006 \\ -0.0006 & 0.0013 \end{bmatrix}$ in the second iteration and become even slightly smaller afterward, meaning that the EKF is significantly more confident that its estimation is accurate, which contradicts the fact that the system is unobservable. In other words, the EKF is not reliable for unobservable systems and gives an inaccurate variance estimation.

Such an inaccurate variance estimation can happen to all nonlinear systems. According to the EKF algorithm, the

updated covariance at step k can be calculated by (4),

$$P_{k|k} = \left(I - \frac{P_{k|k-1} H_k^T H_k}{H_k P_{k|k-1} H_k^T + R_k} \right) P_{k|k-1} \tag{4}$$

Therefore, the variance of $H_k x_{k|k}$ is:

$$\begin{aligned} H_k P_{k|k} H_k^T &= H_k P_{k|k-1} H_k^T - \frac{H_k P_{k|k-1} H_k^T H_k P_{k|k-1} H_k^T}{H_k P_{k|k-1} H_k^T + R_k} \\ &= \frac{H_k P_{k|k-1} H_k^T R_k}{H_k P_{k|k-1} H_k^T + R_k} \end{aligned} \tag{5}$$

Since R_k is positive definite and $H_k P_{k|k-1} H_k^T$ is positive semidefinite, the trace of $H_k P_{k|k} H_k^T$ is smaller than the trace of the measurement covariance matrix R_k. However, H_k is the Jacobian matrix calculated at $x_{k|k-1}$, which is usually not equal to the Jacobian matrix calculated at $x_{k|k}$ and therefore cannot represent the linearized measurement function at $x_{k|k}$. Consequently, EKF underestimates the variance of $H_k x_{k|k}$ and mistakenly believes that the correlation of the states exists in the hyperplanes indicated by the rows of H_k. Such an error will accumulate as the estimation proceeds, making the state covariance matrix inaccurate. The specific error brought by the mismatch between $x_{k|k}$ and H_k is related to the degree of nonlinearity of the system as well as the measurement and process noise. Specifically, when both noises are small, the covariance matrix would collapse to a matrix close to zero in the second iteration, which was precisely what happened in the previous EKF example.

The solution to this problem is simple: we can simply update the measurement Jacobian matrix H according to $x_{k|k}$ before updating the covariance matrix $P_{k|k}$. Back to the previous example, if this extra step is added to the EKF, the covariance matrix will then converge to $P = \begin{bmatrix} 0.2 & -0.4 \\ -0.4 & 0.8 \end{bmatrix}$ instead of a small matrix, meaning that the EKF becomes aware of the fact that the system is unobservable and that its estimation can be inaccurate, just as in the case of KF. However, we also noticed that in some rare cases, adding this extra step can make $Tr(P_{k|k}) > Tr(P_{k|k-1})$ and cause the estimation to diverge in the long run. Therefore, we proposed to update H before updating $P_{k|k}$ only when this makes $P_{k|k}$ positive semidefinite and $Tr(P_{k|k}) < Tr(P_{k|k-1})$.

There are also some other existing KF-based algorithms that can solve the problem of EKF. For example, UKF [17] avoids the calculation of the measurement Jacobian matrix at the cost of higher computational complexity. For another example, the IEKF recalculates the updated states $x_{k|k}$, Kalman gain K, and measurement Jacobian matrix H_k several times until convergence in each time step. However, IEKF cannot guarantee convergence [18], and it also requires a higher computational complexity proportional to the number of iterations. Note that IEKF can only solve the problem of EKF after convergence. When the number of iterations is too small for IEKF to converge, the mismatch between the updated state $x_{k|k}$ and the measurement Jacobian matrix H_k will still exist, causing errors in covariance estimation. Therefore, compared with other existing algorithms, the improvement we proposed solved the problem of EKF with minimal computational complexity.

B. Battery Model

The ECM used in this paper is presented in Fig. 1. It consists of a resistor and an RC pair in addition to the OCV element.

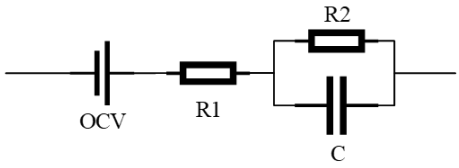

Fig. 1. Equivalent circuit model

In this paper, OCV is considered a function of SOC and SOH. Namely, $OCV = f_{OCV}(SOC, SOH)$. As shown in (6), SOC is defined as the ratio of the cell's remaining capacity (denoted as Q_r) to its present maximum capacity (denoted as Q_{max}).

$$SOC = \frac{Q_r}{Q_{max}} \tag{6}$$

The differential form of (6) is shown in (7), which suggests that the SOC can be estimated by taking the integral of the current.

$$dSOC = \frac{Idt}{Q_{max}} \tag{7}$$

SOH, on the other hand, as shown in (8), is defined as the ratio of the cell's present maximum capacity to its initial maximum capacity (also often referred to as the nominal capacity, denoted as Q_{no}). Since the maximum capacity changes very slowly, the SOH can be considered a constant during a single cycle.

$$SOH = \frac{Q_{max}}{Q_{no}} \tag{8}$$

Back to the system model shown in Fig. 1, If we select the remaining capacity (in As), capacitor voltage (U_c, in V), and present maximum capacity (in As) as the states, current (I, in A) as the input, and terminal voltage (U_{ter}, in V) as the output, the discrete state-space representation of the system can be written as (9).

$$\begin{cases} \begin{bmatrix} Q_{r,k} \\ U_{c,k} \\ Q_{max,k} \end{bmatrix} = F \begin{bmatrix} Q_{r,k-1} \\ U_{c,k-1} \\ Q_{max,k-1} \end{bmatrix} + BI_k \\ U_{ter,k} = f_{OCV}(\frac{Q_{r,k}}{Q_{max,k}}, \frac{Q_{max,k}}{Q_{no}}) + U_{c,k} + R_1 I_k \end{cases} \tag{9}$$

where B and F are two constant matrices defined by (10), in which Δt is the time interval between two steps.

$$F = \begin{bmatrix} 1 & 0 & 0 \\ 0 & e^{\frac{-\Delta t}{R_2 C}} & 0 \\ 0 & 0 & 1 \end{bmatrix}, B = \begin{bmatrix} \Delta t \\ R_2 - R_2 e^{\frac{-\Delta t}{R_2 C}} \\ 0 \end{bmatrix} \tag{10}$$

Notice that (9) follows the general nonlinear system model represented by (1). By comparing the two equations, the following correspondence can be found.

$$\begin{cases} \boldsymbol{x_k} = \begin{bmatrix} Q_{r,k} \\ U_{c,k} \\ Q_{max,k} \end{bmatrix}, u_k = I_k \\ f(\boldsymbol{x_{k-1}}, u_k) = F\boldsymbol{x_k} + Bu_k \\ z_k = U_{ter,k} \\ h(\boldsymbol{x_k}, u_k) = f_{OCV}(\frac{Q_{r,k}}{Q_{max,k}}, \frac{Q_{max,k}}{Q_{no}}) + U_{c,k} + R_1 I_k \end{cases} \tag{11}$$

Therefore, an EKF can be constructed to estimate the states of the system. According to Algorithm 1, the only missing pieces are the process noise covariance matrix Q_k and the measurement noise covariance matrix R_k, the calculation of which will be introduced in the next section.

Finally, it is worth mentioning that the definition of the system states is not unique. For example, an alternative definition is to replace the state "remaining capacity" with the state "SOC". The reason that we chose the present definition was to make the state-transition matrix F constant so that the nonlinearity only appears in the output function.

C. Rigorous Calculation of the Process Noise and the Measurement Noise

In the EKF, the process noise and measurement noise are considered zero-mean Gaussian noise with covariance matrices Q and R, respectively. In battery state estimation, past literature that uses KF or EKF usually considers Q and R to be constant matrices and sometimes even fine-tune their values to get the best estimation result [12]. However, after a closer look at the state-space representation in (9) and a careful examination of the error sources, we realized that a more rigorous and objective way to calculate the process noise and measurement noise is to make them dynamic and related to the states and inputs.

The error sources in the state transition function in (9) include the inaccurate current measurement and the inaccurate ECM parameters. The latter refers to the parameters R_2 and $1/(R_2C)$, which are modeled as constants but are actually changing during charge and discharge. Additionally, since the first-order RC model cannot fully capture the dynamics of a battery, the "actual" value of these ECM parameters can change even when the current is zero.

The expected error caused by each of these error sources is derived under the following assumptions:

- **[A1]:** We assumed that the error caused by each error source is independent of each other and is independent of the states.
- **[A2]:** We used the first-order Taylor series to approximate the nonlinear functions of random variables. Specifically, function f of a random variable X is approximated at the point $E(X)$ as $f(X) = f(E(X)) + f'(E(X))(X - E(X))$, and its variance is therefore approximated as $(f'(E(X)))^2\sigma_X^2$. For example, if the random variable a has a mean of a_0 and a variance of σ_a^2, then the random variable e^a can be approximated by $e^{a_0}(1 + a - a_0)$, and its variance can be calculated by $e^{2a_0}\sigma_a^2$
- **[A3]:** We assumed that all the errors have zero mean and follow the Gaussian distribution.

Denote the standard deviation of current measurement, R_2, and $1/(R_2C)$ as σ_I, σ_{R_2} and $\sigma_{1/(R_2C)}$, respectively. Based on the three assumptions and the state-space function in (9), the process noise covariance matrix at step k can be formulated as (12). Note that the state-space function for Q_{max} is assumed to be accurate because the SOH is considered constant during a single cycle.

$$Q_k = \begin{bmatrix} Q_{1,1} & Q_{1,2} & 0 \\ Q_{1,2} & Q_{2,2} & 0 \\ 0 & 0 & 0 \end{bmatrix} \tag{12}$$

where

$$\begin{cases} Q_{1,1} = \Delta t^2 \sigma_I^2 \\ Q_{1,2} = \Delta t (R_2 - R_2 e^{-\frac{\Delta t}{R_2 C}}) \sigma_I^2 \\ Q_{2,2} = \Delta t^2 e^{-\frac{2\Delta t}{R_2 C}} (U_{c,k-1} - R_2 I_k)^2 \sigma_{1/(R_2C)}^2 \\ \quad + (R_2 - R_2 e^{-\frac{\Delta t}{R_2 C}})^2 \sigma_I^2 + I_k^2 (1 - e^{-\frac{\Delta t}{R_2 C}})^2 \sigma_{R_2}^2 \end{cases} \tag{13}$$

As for the measurement function in (9), the error sources are the inaccurate OCV function (because the fitted OCV function may be different from the actual OCV function), the voltage measurement noise, the inaccurate internal resistance R_1, and the inaccurate current measurement. Denote the standard deviation of the OCV function and the voltage measurement as σ_{OCV} and σ_V, respectively. Taking assumptions **[A1]** and **[A3]**, the variance of the measurement function can be formulated as (14).

$$R_k = \sigma_{OCV}^2 + \sigma_V^2 + I_k^2 \sigma_{R_1}^2 + R_1^2 \sigma_I^2 \tag{14}$$

By using (12)-(14) to quantify the process noise and measurement noise, we proposed an improved EKF algorithm to estimate the battery SOC and SOH, which is shown in Algorithm 2. The basic architecture of the algorithm is the same as Algorithm 1, except that we added an extra step to update the measurement Jacobian matrix H after the state update for the reasons illustrated in Section II-A.

Once the states and the covariance matrix are estimated, the final step is calculating the expected value and confidence interval of SOC and SOH. The former can be calculated by using (6) and (8) after the states Q_r and Q_{max} are estimated. As for the variance, SOH is only related to the state Q_{max}, so its variance can be calculated by (15). However, as for SOC, its variance cannot be directly calculated because it is the quotient of two random variables. Therefore, assumptions **[A2]-[A3]** are again taken to linearize (6), and the variance of SOC is approximated by (16).

$$\sigma_{SOH}^2 = \frac{\sigma_{3,3}^2}{Q_{no}^2} \tag{15}$$

$$\sigma_{SOC}^2 = \frac{1}{Q_{max}^2}\sigma_{1,1}^2 + \frac{Q_r^2}{Q_{max}^4}\sigma_{3,3}^2 - \frac{2Q_r}{Q_{max}^3}\sigma_{1,3}^2 \tag{16}$$

where $\sigma_{i,j}$ is the element in the i^{th} row and j^{th} column of the covariance matrix P.

Algorithm 2 The proposed SOC + SOH estimation algorithm

Inputs: $\boldsymbol{x_0}, P_0, I_k, U_{ter,k}$

$k \leftarrow 0$

while $k < length(\boldsymbol{u})$ **do**

$k \leftarrow k + 1$

State prediction $\boldsymbol{x_k} \leftarrow F\boldsymbol{x_{k-1}} + BI_k$ (see (10) for details)

Calculate the process noise Q_k by using (12)

Covariance prediction $P_k \leftarrow FP_{k-1}F^T + Q_k$

Calculate the residual $y_k \leftarrow U_{ter,k} - h(\boldsymbol{x_k}, I_k)$ (see (11) for details)

Calculate the measurement Jacobian matrix H_k

Calculate the measurement noise R_k by using (14)

Calculate the Kalman gain $K_k \leftarrow \frac{P_k H_k^T}{H_k P_k H_k^T + R_k}$

State update $\boldsymbol{x_k} \leftarrow \boldsymbol{x_k} + K_k y_k$

Update the measurement Jacobian matrix H_k

Covariance update $P_k \leftarrow (I - K_k H_k)P_k$

$SOC_k \leftarrow \boldsymbol{x_k}(1)/\boldsymbol{x_k}(3)$

$SOH_k \leftarrow \frac{\boldsymbol{x_k}(3)}{Q_{no}}$

Calculate σ^2_{SOC} by using (16)

Calculate σ^2_{SOH} by using (15)

Output $SOC_k, SOH_k, \sigma^2_{SOC}, \sigma^2_{SOH}$

end while

D. The Shift of the OCV Curve with Respect to SOH

A unique feature of our SOC & SOH estimation algorithm is that we consider OCV as a function of both SOC and SOH instead of just SOC. Although some literature found that the OCV curve is affected by the SOH [19], [20], most of the existing literature that used EKF to do battery state estimation didn't consider such an effect. To study whether such consideration is necessary, we aged six lithium-ion batteries with NCM cathode (Model: ICR18650-22F) from 100% SOH to 80% SOH and recorded their OCV throughout the aging process. For each OCV curve, we performed a ninth-order polynomial fitting. The OCV curves with respect to different SOH are shown in Fig. 2. The partial derivative of the curves with respect to SOC is shown in Fig. 3.

At first glance, according to Fig. 2, the effect of SOH on the OCV is not very strong. However, in EKF, the estimation of the SOH is related to the measurement Jacobian matrix H, which is almost proportional to $\frac{\partial OCV}{\partial SOC}$. Since the correlation between $\frac{\partial OCV}{\partial SOC}$ and the SOH is very strong, especially at around 40% SOC and above 85% SOC, ignoring the effect of SOH can make the estimation result inaccurate, and the magnitude of such an effect is related to the measurement noise and the present SOC.

III. Simulation and Discussion

A. Simulation Setup

Two different simulation profiles are used to validate the effectiveness of the proposed algorithm. The first profile is a constant-current (CC) charge & discharge profile. In this profile, the cell starts with 100% SOC and is firstly discharged at a constant C-rate of 1C to 0% SOC. Then, after a 300-second rest, the cell is charged at a constant C-rate of 1C to 100% SOC. The C-rate is defined by the cell's present maximum capacity, so when $Q_{no} = 2.2$ Ah and the SOH is 90%, a 1C C-rate corresponds to 2.2*0.9 A. The second profile is an Urban Dynamometer Driving Schedule (UDDS) profile, which aims to simulate the current of an EV during a driving cycle. In this profile, the cell starts with 100% SOC and decreases to about 58% SOC at the end of the profile. In both simulations, the initial states ($\boldsymbol{x_0}$) and the initial covariance matrix (P_0) are shown in (17), while the true SOH is 90%.

$$\boldsymbol{x_0} = \begin{bmatrix} 0.855Q_{no} \\ 0 \\ 0.95Q_{no} \end{bmatrix}, P_0 = \begin{bmatrix} 0.0025Q_{no}^2 & 0 & 0 \\ 0 & 0 & 0 \\ 0 & 0 & 0.0025Q_{no}^2 \end{bmatrix} \quad (17)$$

All the other parameter setups are summarized in Table I. All the noise terms (including the noise of the measurement and the noise of the parameters) are assumed to be independently and normally distributed in the simulation.

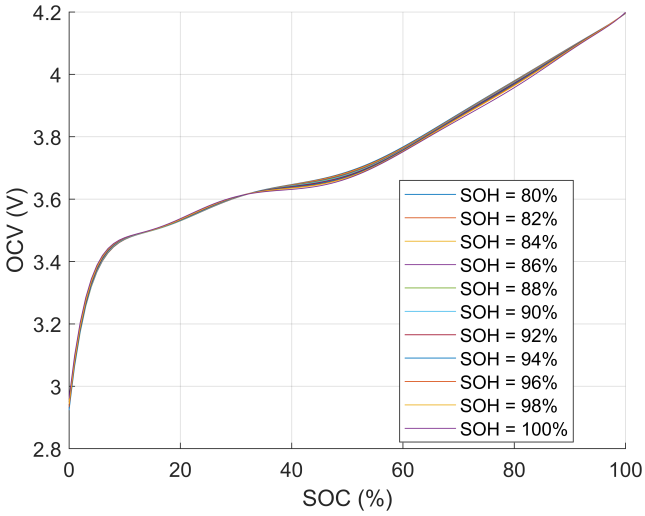

Fig. 2. The experimentally measured open circuit voltage (OCV) curve at various state-of-health (SOH).

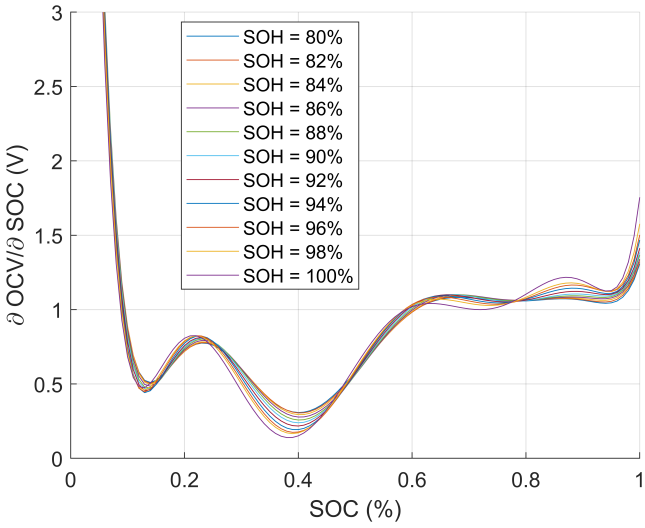

Fig. 3. The partial derivative of the OCV w.r.t. SOC at various SOH.

TABLE I

SIMULATION PARAMETER SETUP

Parameter	Q_{no}	R_1	R_2	$1/(R_2C)$	σ_{R1}
Value	2.2 Ah	80 mΩ	50 mΩ	8e-3 Hz	8 mΩ
Parameter	σ_{R2}	$\sigma_{1/(R_2C)}$	σ_I	σ_{OCV}	σ_V
Value	5 mΩ	8e-4 Hz	0.5 mA	4 mV	1 mV

B. Constant-current Discharge & Charge

The simulation result for the CC charge & discharge profile is shown in Fig. 4 and 5. Because the estimation error is small compared to the absolute value, only the estimation error (defined as the difference between the estimated state and the true state) is plotted in the two figures. In both figures, the estimation error upper and lower bound are defined as the difference between the 2-sigma bound (95.4% confidence interval bound) and the estimated value, representing the algorithm's degree of confidence in its estimation. The standard deviation of the SOC and SOH estimation is calculated using (15) and (16).

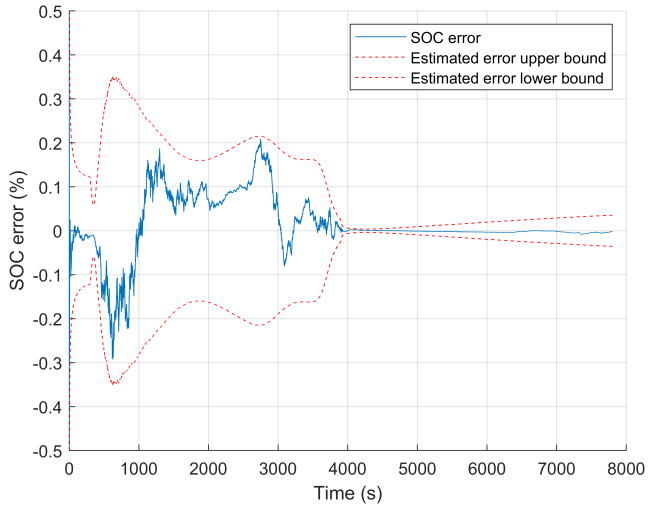

Fig. 4. SOC estimation error using our algorithm (constant current)

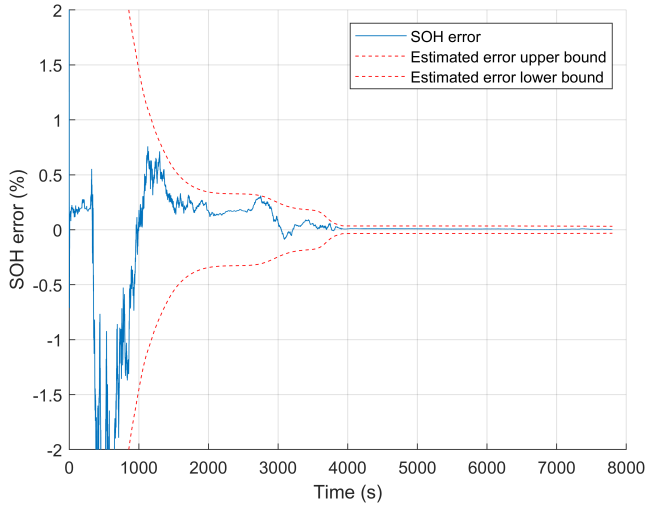

Fig. 5. SOH estimation error using our algorithm (constant current)

From the results, we can see that the magnitude of the error is very small (<0.1% for both SOC and SOH after convergence) and is bounded by the 95.4% confidence interval most of the time, indicating that the algorithm can provide not only accurate state estimation but also accurate variance estimation as well. In other words, the proposed EKF is self-aware of its performance. Additionally, the error of both SOC and SOH estimation can decrease from 5% to 1% within 15 minutes, suggesting that the convergence speed of the algorithm is also high.

C. Urban Dynamometer Driving Schedule

The simulation result for the UDDS profile is shown in Fig. 6 and 7. The conclusion here is similar - the magnitude of the error is very small (<0.2% for both SOC and SOH after convergence) and is bounded by the 95.4% confidence interval most of the time. The convergence speed is slightly lower than the CC profile, but the error can still decrease to 1% within 30 minutes.

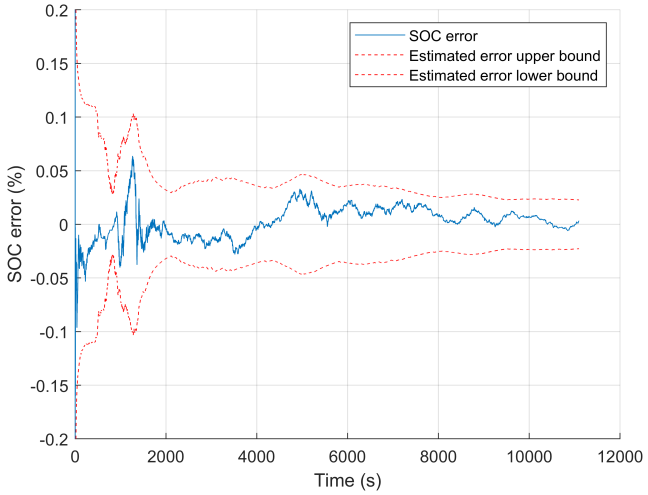

Fig. 6. SOC estimation error using our algorithm (UDDS)

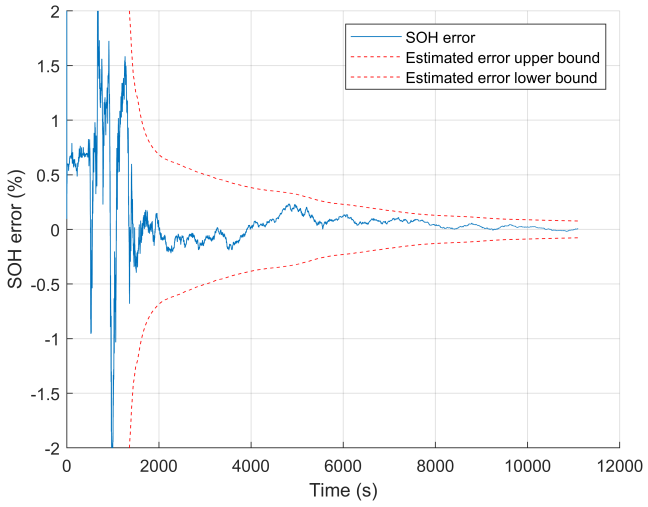

Fig. 7. SOH estimation error using our algorithm (UDDS)

D. Comparison

To test whether the suggested three improvements really make the estimation better, we did an ablation study to quantify the contribution of each improvement. Specifically, we remove one improvement from our algorithm at a time until the algorithm degrades to the conventional EKF and compare the results in terms of the computational complexity (shown in Table II), SOC and SOH estimation accuracy (also shown in Table II), and the accuracy of the estimated confidence interval (shown in Fig. 8). All the data in Table II and Fig. 8 are the average of one thousand simulations, which guarantees the statistical significance of the results. In Table II and Fig. 8, Improvement 1 refers to the extra step we added to the EKF algorithm introduced in Section II-A, where output Jacobian H_k is recalculated after the state update step (if this guarantees $Tr(P_{k|k}) > Tr(P_{k|k-1})$ and $P_{k|k}$ to be positive semidefinite). When Improvement 1 is removed, we remove the extra step. Improvement 2 refers to the rigorous calculation of process noise and the measurement noise introduced in Section II-C. When Improvement 2 is removed, the process noise covariance matrix and the measurement noise covariance matrix (which are previously calculated by (12-14)) are replaced by two constant matrices shown in (18),

$$Q_k = \begin{bmatrix} \Delta t^2 \sigma_I^2 & 0 & 0 \\ 0 & (0.1 I_{rms} R_2)^2 & 0 \\ 0 & 0 & 0 \end{bmatrix}, R_k = \sigma_{OCV}^2 + \sigma_V^2 \tag{18}$$

where I_{rms} is the RMS current in the profile. Improvement 3 refers to the consideration of the shift of the OCV curve to SOH. When Improvement 3 is removed, the OCV is considered only related to the SOC, and the OCV function measured at 100% SOH is used as the measurement function.

TABLE II

PERFORMANCE COMPARISON OF DIFFERENT EKF-BASED METHODS

Algorithms	SOC RMS error (%)		SOH RMS error (%)		Avg. run time (ms)
	CC	UDDS	CC	UDDS	
EKF + Imp. 1+2+3	0.141	0.101	0.500	0.615	85.5
EKF + Imp. 2+3	0.148	0.114	0.648	0.841	53.0
EKF + Imp. 3	0.238	0.165	1.665	1.464	52.6
EKF	1.079	1.350	3.557	6.752	36.9

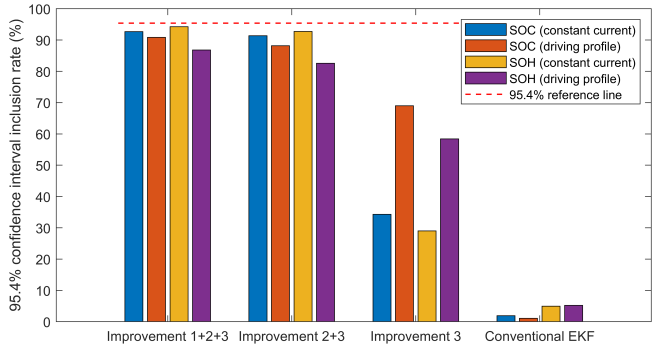

Fig. 8. The accuracy of the confidence interval given by different EKF-based algorithms

In Table II, "SOC RMS error" and "SOH RMS error" are the RMS of the estimation error taken from all the time steps, which represent the accuracy of different algorithms. In Fig. 8, each bar shows the probability that the actual state is within the 2-sigma confidence interval. Under ideal conditions, i.e., Gaussian zero-mean noise and linear dynamics, this probability should be 95.4%, so the closeness of the bars to 95.4% indicates the accuracy of the confidence interval. Interestingly, as our new algorithm gradually degrades to the conventional EKF algorithm, the actual error keeps increasing while the confidence interval inclusion rate shrinks. It suggests that the proposed algorithm not only has the highest SOC and SOH estimation accuracy but also gives the most accurate confidence interval estimation.

UKF is another KF-based state estimation algorithm that can be applied to nonlinear systems. UKF is known to have a higher accuracy than EKF because it addresses the approximation issues of the EKF at the cost of a higher computational complexity. Since this paper is about an improved EKF algorithm, it would be interesting to compare the results against UKF, which can also be called an improved EKF algorithm. Since the UKF algorithm does not need the calculation of the Jacobian matrix of the measurement function, the proposed Improvement 1 cannot be applied to it. In contrast, the other two improvements can still be applied when using the UKF to estimate the battery SOC and SOH. The average performance of different UKF algorithms in a thousand simulations is shown in Table III and Fig. 9.

TABLE III

PERFORMANCE COMPARISON OF DIFFERENT UKF-BASED METHODS

Algorithms	SOC RMS error (%)		SOH RMS error (%)		Avg. run time (ms)
	CC	UDDS	CC	UDDS	
UKF + Imp. 2+3	0.140	0.099	0.586	0.530	328.8
UKF + Imp. 2	1.125	1.369	3.197	6.713	329.8
UKF + Imp. 3	4.334	0.697	5.802	2.549	328.8
UKF	3.979	1.408	5.425	5.024	326.4

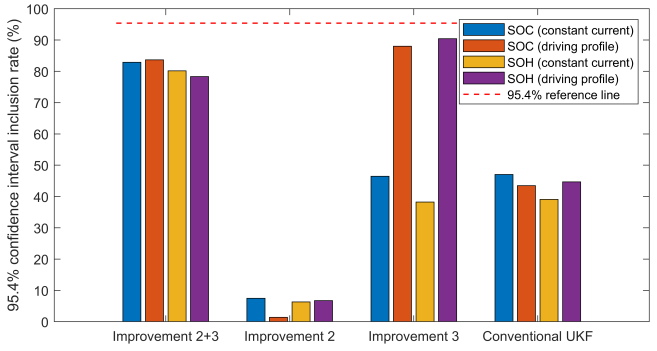

Fig. 9. The accuracy of the confidence interval given by different UKF-based algorithms

From Table III and Fig. 9, we can see that the proposed two improvements can also significantly improve the performance of the UKF algorithm when used together. Additionally, by comparing Table III against Table II, we can see that the UKF algorithm (with Improvements 2 and 3) is indeed better than the conventional EKF algorithm

(with Improvements 2 and 3), and is almost as good as than our improved EKF algorithm (with Improvement 1, 2, and 3). Note that our proposed improvements add minimal computational complexity to the EKF and have significantly less computational complexity than the UKF. Namely, the run time of our improved EKF algorithm (with all three improvements) is 61% longer than the EKF with Improvement 2+3, while the run time of the UKF algorithm (with Improvements 2+3) is 520% longer than the EKF with Improvements 2+3. Therefore, we conclude that Improvement 1 helps EKF to be as good as, or even better than (in terms of variance estimation), the UKF algorithm while maintaining EKF's advantage of low complexity.

Interestingly, in Fig. 9, the UKF with only Improvement 2 gives the worst confidence interval estimation. This result is seemingly contradictory to the fact that Improvement 2 is directly related to the accurate quantification of the process noise and measurement noise, and it should theoretically increase the accuracy of the confidence interval estimation. However, in the simulation, the standard deviation of the OCV curve σ_{OCV} is assumed to be the same regardless of whether the OCV curve is related to the SOH. When Improvement 3 is not implemented, the error of the OCV curve would be significantly higher than expected because the relationship between the OCV and SOH is ignored. Therefore, Improvement 2 can only show its value when used together with Improvement 3. This again shows the importance of considering battery aging while estimating the SOC because otherwise, the error of the OCV curve can be underestimated, and the algorithm's performance will be compromised after the battery ages.

IV. Acknowledgment

M. Borah in this work is supported by Fulbright fellowship grant and SAFT.

V. CONCLUSIONS

A new SOC and SOH co-estimation method based on an improved EKF algorithm is presented in this paper. Compared with the conventional EKF algorithm, the new algorithm gives more accurate state estimation and variance estimation by (1) adding an extra step to the EKF algorithm to prevent over-confident covariance estimation, (2) considering the variance of process noise and measurement noise to be changing and estimating their values in real-time, and (3) considering the OCV curve as a function of both SOC and SOH. The method is validated in two different current profiles in the simulation, giving very accurate state estimations and confidence interval estimation in both cases. Finally, an ablation study shows that all three suggested improvements are beneficial for giving an accurate state and covariance estimation. With all the improvements, the proposed EKF algorithm can even be slightly better than the UKF algorithm despite the latter being computationally more complex. Future work includes experimental validation on different cells and different current profiles.

References

[1] J. Shi, M. Tian, S. Han, T.-Y. Wu, and Y. Tang, "Electric vehicle battery remaining charging time estimation considering charging accuracy and charging profile prediction," Journal of Energy Storage, vol. 49, p. 104132, May 2022, doi: 10.1016/j.est.2022.104132.

[2] A. Eddahech, O. Briat, and J.-M. Vinassa, "Determination of lithium-ion battery state-of-health based on constant-voltage charge phase," Journal of Power Sources, vol. 258, pp. 218–227, Jul. 2014, doi: 10.1016/j.jpowsour.2014.02.020.

[3] S. Jiang and Z. Song, "A review on the state of health estimation methods of lead-acid batteries," Journal of Power Sources, vol. 517, p. 230710, Jan. 2022, doi: 10.1016/j.jpowsour.2021.230710.

[4] S. Jiang and Z. Song, "Estimating the State of Health of Lithium-Ion Batteries with a High Discharge Rate through Impedance," Energies, vol. 14, no. 16, Art. no. 16, Jan. 2021, doi: 10.3390/en14164833.

[5] A. M. Bizeray, S. Zhao, S. R. Duncan, and D. A. Howey, "Lithium-ion battery thermal-electrochemical model-based state estimation using orthogonal collocation and a modified extended Kalman filter," Journal of Power Sources, vol. 296, pp. 400–412, Nov. 2015, doi: 10.1016/j.jpowsour.2015.07.019.

[6] S. Huang and G. Dissanayake, "Convergence and Consistency Analysis for Extended Kalman Filter Based SLAM," IEEE Transactions on Robotics, vol. 23, no. 5, pp. 1036–1049, Oct. 2007, doi: 10.1109/TRO.2007.903811.

[7] Z. Zhu and C. Taylor, "Conservative Uncertainty Estimation in Map-Based Vision-Aided Navigation," IEEE Transactions on Aerospace and Electronic Systems, vol. 53, no. 2, pp. 941–949, Apr. 2017, doi: 10.1109/TAES.2017.2667278.

[8] Y. Wang et al., "A comprehensive review of battery modeling and state estimation approaches for advanced battery management systems," Renewable and Sustainable Energy Reviews, vol. 131, p. 110015, Oct. 2020, doi: 10.1016/j.rser.2020.110015.

[9] Fang, Huazhen, et al. "State of charge estimation for lithium-ion batteries: An adaptive approach." Control Engineering Practice 25 (2014): 45-54.

[10] G. L. Plett, "Extended Kalman filtering for battery management systems of LiPB-based HEV battery packs: Part 1. Background," Journal of Power Sources, vol. 134, no. 2, pp. 252–261, Aug. 2004, doi: 10.1016/j.jpowsour.2004.02.031.

[11] W. Xu et al., "A novel adaptive dual extended Kalman filtering algorithm for the Li-ion battery state of charge and state of health co-estimation," International Journal of Energy Research, vol. 45, no. 10, pp. 14592–14602, 2021, doi: 10.1002/er.6719.

[12] Maheshwari, A., and S. Nageswari. "Effect of Noise Covariance Matrices on State of Charge Estimation Using Extended Kalman Filter." IETE Journal of Research (2022): 1-12.

[13] M. Einhorn, F. V. Conte, C. Kral, and J. Fleig, "A Method for Online Capacity Estimation of Lithium Ion Battery Cells Using the State of Charge and the Transferred Charge," IEEE Transactions on Industry Applications, vol. 48, no. 2, pp. 736–741, Mar. 2012, doi: 10.1109/TIA.2011.2180689.

[14] SA. Marongiu, N. Nlandi, Y. Rong, and D. U. Sauer, "On-board capacity estimation of lithium iron phosphate batteries by means of half-cell curves," Journal of Power Sources, vol. 324, pp. 158–169, Aug. 2016, doi: 10.1016/j.jpowsour.2016.05.041.

[15] C. R. Birkl, M. R. Roberts, E. McTurk, P. G. Bruce, and D. A. Howey, "Degradation diagnostics for lithium ion cells," Journal of Power Sources, vol. 341, pp. 373–386, Feb. 2017, doi: 10.1016/j.jpowsour.2016.12.011.

[16] L. Wang, D. Lu, Q. Liu, L. Liu, and X. Zhao, "State of charge estimation for LiFePO4 battery via dual extended kalman filter and charging voltage curve," Electrochimica Acta, vol. 296, pp. 1009–1017, Feb. 2019, doi: 10.1016/j.electacta.2018.11.156.

[17] S. J. Julier and J. K. Uhlmann, "Unscented filtering and nonlinear estimation," in Proceedings of the IEEE, vol. 92, no. 3, pp. 401-422, March 2004, doi: 10.1109/JPROC.2003.823141.

[18] Havlík, Jindřich, and Ondřej Straka. "Performance evaluation of iterated extended Kalman filter with variable step-length." Journal of Physics: Conference Series. Vol. 659. No. 1. IOP Publishing, 2015.

[19] Lavigne, Loïc, et al. "Lithium-ion Open Circuit Voltage (OCV) curve modelling and its ageing adjustment." Journal of Power Sources 324 (2016): 694-703.

[20] Birkl, Christoph R., et al. "Degradation diagnostics for lithium ion cells." Journal of Power Sources 341 (2017): 373-386.